Supplementary material – Exciton-phonon coupling in the UV absorption and emission spectra of bulk hexagonal boron nitride

Fulvio Paleari,[1] Henrique P. C. Miranda,[1,2] Alejandro Molina-Sánchez,[3] and Ludger Wirtz[1]

[1] *Physics and Materials Science Research Unit, University of Luxembourg, 162a avenue de la Faïencerie, L-1511 Luxembourg, Luxembourg*

[2] *Institute of Condensed Matter and Nanosciences, Université catholique de Louvain, Chemin des étoiles 8, bte L7.03.01, 1348, Louvain-la-Neuve, Belgium*

[3] *Institute of Materials Science (ICMUV), University of Valencia, Catedrático Beltrán 2, E-46980 Valencia, Spain*

(Dated: April 5, 2019)

I. METHODS

The supercell[1] used in our calculations is represented in Fig. S1 and compared with the unit cell. The comparison between the respective reciprocal-space Brillouin zones (BZ) is also shown, emphasizing the folding of the q-point $\bar{q}$ (given in fractional coordinates as $(1/3, -1/6, 0)$) onto Γ in the supercell case (note that both $\bar{q}$ and $-\bar{q}$ are folded onto Γ in this way).

The DFT ground state calculations were performed with Quantum ESPRESSO[2] using LDA[3] norm-conserving pseudopotentials[4] with a kinetic energy cutoff at 110 Ry. The phonon frequencies and eigenmodes

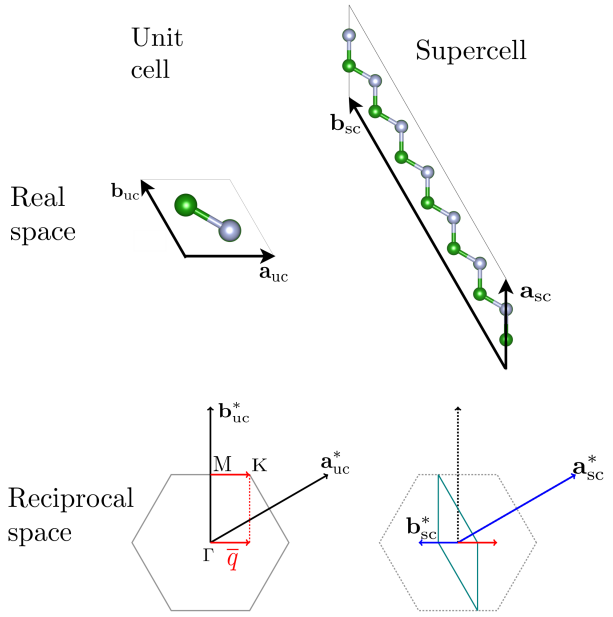

FIG. S1. Top: representations of the hBN unit cell (uc) and non-diagonal supercell (sc) used in our calculations (boron is green, nitrogen is gray). Bottom: schemes of the reciprocal-space BZ in the two cases (the BZ borders are in gray and teal, respectively), showing that in the first Brillouin zone of the supercell, the momentum $\bar{q}$ is folded back onto the Γ point.

were computed with density functional perturbation theory (DFPT),[5] using a q-point grid sampling of $18\times18\times6$. The G_0W_0 and semi-self-consistent GW_0 ($scGW_0$) corrections to the band energies were obtained with the YAMBO code[6] for the unit cell, using the plasmon-pole approximation for the dynamical screening. The direct and indirect gaps were converged with a $18\times18\times6$ k-point grid, summing 160 and 280 states for the screening function and the Green's function, respectively. The corrections were computed for the last 4 valence bands and the first 6 conduction bands. The $scGW_0$ amounts to an additional opening of the band gap by 0.22 eV with respect to the single G_0W_0 calculation.[7] The fully converged result was subsequently used to construct a k-dependent scissor operator in such a way that, when applied to the supercell, it would yield exactly the same optical absorption spectrum as the unit cell (here we neglect the changes in the GW corrections due to lattice displacements). The exciton energies E^s and wave functions Φ^S were computed with YAMBO by solving the Bethe-Salpeter equation (BSE) with RPA static screening and the Tamm-Dancoff approximation, including the GW-corrected band structures. The Bethe-Salpeter equation in the supercell is solved iteratively in the YAMBO code using the SLEPC library[8] for the first 600 eigenvalues and eigenvectors. The macroscopic dielectric function $\varepsilon^{(0)}(\omega)$ was computed using the modified response function where the long-range Fourier component is removed.[9] Its resonant part can be written as:

$$\varepsilon^{(0)}(\omega) = 1 - \frac{8\pi}{N_k V_R} \sum_S \frac{|T^S|^2}{\hbar\omega - E^S + \mathrm{i}\eta}. \qquad \text{(S1)}$$

Here, N_k is the number of k-points in the Brillouin zone sampling and V_R the BZ volume. The term in the numerator, $T^S = \sum_{kcv} \Phi^S_{cvk} \langle ck| \mathbf{e}\cdot\hat{\mathbf{D}} |vk\rangle$, is the oscillator strength of exciton S. It is a linear combination of optical matrix elements in the dipole approximation ($\mathbf{e}$ is the light polarization direction), describing direct transitions from an occupied state v to an unoccupied one c, weighted by the corresponding components of the excitonic wave function. In the unit cell, a reasonably converged calculation of the static screening can be obtained by considering an $18\times18\times6$ k-point grid and summing 250 bands. However, the energy window close to the absorption edge is already converged with a $12\times12\times4$ sam-

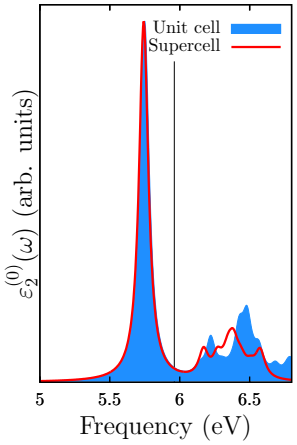

FIG. S2. The imaginary part of the dielectric functions are plotted for the hBN unit cell (blue, DFT-GW-BSE calculation on fine k-point grid) and non-diagonal supercell (red, DFT-scissor-BSE calculation on coarse k-point grid). Only the first 480 states are included in the iterative solution of the BSE in the supercell. The black vertical line is at the energy of the indirect quasiparticle band gap. Both spectra have a broadening parameter of 0.04 eV. Difference in the spectra (due to finite k-point samplings) only occur in the energy region above the band gap. In the relevant energy region below the band gap, both spectra are identical.

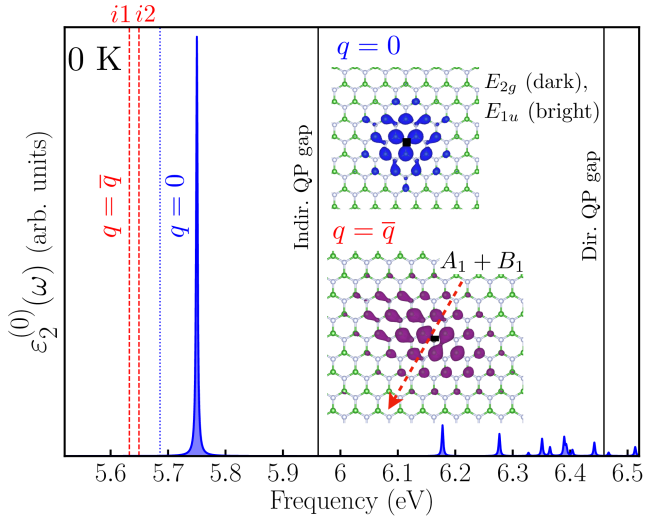

FIG. S3. Equilibrium supercell calculation. The imaginary part of the dielectric function including only transitions at $q = 0$ ($\mathrm{Im}\,\varepsilon^{(0)}(\omega)$ in the text) is shown in blue. The peak broadenings are set to 1.5 meV for the temperature of 0 K. The vertical black lines denote the quasiparticle indirect and direct gaps, while the dotted blue line indicates the position of the dark E_{2g} exciton with $q = 0$. The dashed red lines indicate the positions of the A_1 and B_1 excitons at $\overline{q}$ (labeled $i1$ and $i2$, respectively). The excitonic wave functions are plotted (intensities only) in the insets: blue for the $q = 0$ pair, and purple for $q = \overline{q}$ ones (the dashed red arrow labeling the $\overline{q}$ direction). Here the hole (black square) is fixed on top of a nitrogen atom, and the resulting electronic density is displayed.

pling. As the non-diagonal supercell contains 6 times the atoms of the unit cell, the convergence parameters were changed accordingly, using a $12 \times 2 \times 4$ k-point grid, and including enough states in the Bethe-Salpeter kernel to span the transition energy region relevant for the absorption edge. The static screening was computed summing $1.2 \cdot 6 \cdot 250$ bands. The factor 1.2 is a safety margin to account both for the folded bands from the zone edge and for spurious finite-q bands (see Fig. S2 for a comparison of the optical absorption spectra $\mathrm{Im}\,\varepsilon^{(0)}(\omega)$ between unit cell and supercell). The normalised phonon displacements (rescaled by the square root of the atomic masses) were used to compute the finite-difference derivatives. A global scaling factor was multiplied by the displacements and converged to 0.0025 Å, which is just above the threshold of numerical noise. The harmonic behaviour of $\varepsilon(\omega)$ with respect to the scaling factor was numerically verified.

II. EQUILIBRIUM RESULTS ON THE SUPERCELL

The result of a BSE calculation in the supercell with atoms fixed at their equilibrium positions is shown in Fig. S3. The energy separations between direct and indirect band gaps, as well as with low-lying $q = 0$ and finite-q excitonic states, are emphasized by vertical lines. The first $q = 0$ exciton at 5.7 eV (dashed blue vertical line) is dark, while the second one at 5.75 eV (main blue peak) is optically active. The intensities of their wave functions $\Psi(\mathbf{r_e}, \mathbf{r_h})$ are almost identical. The one of the bright exciton is represented in blue in the inset of Fig. S3. Both electron and hole mostly lie in the same layer. Two finite-q excitonic states appear below the direct ones: they are labeled $i1$ and $i2$ (dashed red lines). The wave function intensities of the two indirect excitons are very similar. One of them is displayed in purple in the second inset of Fig. S3, showing again a mostly planar distribution. Although the wave function in the fixed-hole representation looks approximately distorted along the armchair lattice direction, the full wave function is actually symmetric with respect to the zigzag direction (parallel to the $\overline{q}$-vector) upon rotation around the principal axis of the C_{2v} symmetry group which is oriented in-plane along the $\overline{q}$ direction (see also Section VI).

III. POSITION OF THE DIRECT BAND GAP

The direct quasiparticle band gap in bulk hBN is traditionally identified at the so-called T_1 point.[10] From Fig. 1 of the main text, we see that this point lies close to K, along the ΓK symmetry line (to be precise:

$|\mathbf{T_1}-\mathbf{K}| \simeq 1/6|\mathbf{K}-\mathbf{\Gamma}|$). However, there are other three points that give a comparable band gap: M, T_2 (along the MK line: $|\mathbf{T_2}-\mathbf{K}| \simeq 1/3|\mathbf{K}-\mathbf{M}| = 1/6|\mathbf{K}-\mathbf{\Gamma}|$), and H, the high-symmetry point directly above K along the out-of-plane direction. In our GW calculations, the band gaps at these points lie in a small 0.1 eV energy interval (with $E_g^H < E_g^{T_2} < E_g^M < E_g^{T_1}$), which is the accuracy of the GW method. Since we know that GW underestimates the true quasiparticle corrections in hBN, we have to assume that the relative energy differences between these band gaps may change with more refined approximations and/or more accurate calculations. In the main text, we "average" the true position of the top of the valence band from "around" K to exactly K, by taking $\overline{q} = |\mathbf{K}-\mathbf{M}| = 0.5|\mathbf{K}-\mathbf{\Gamma}|$ as the momentum transfer corresponding to the indirect gap.

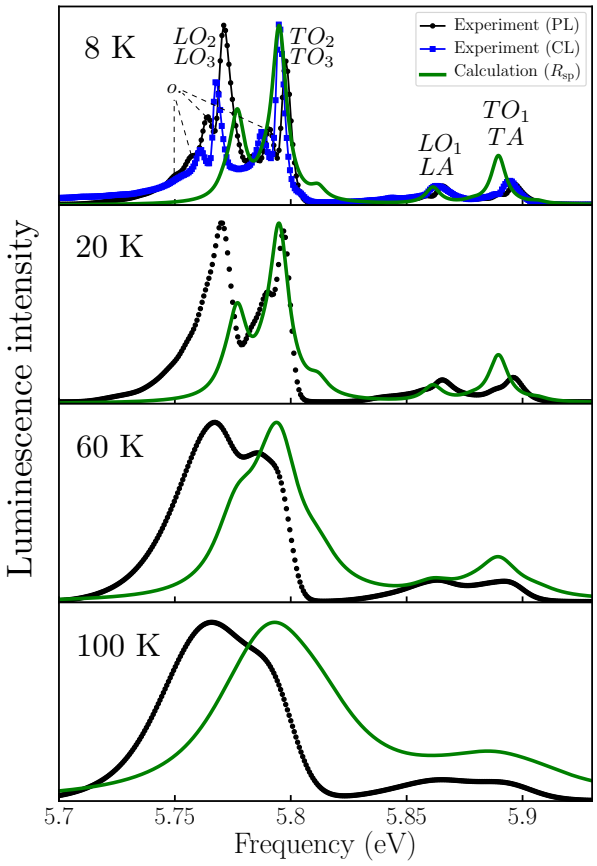

FIG. S4. Temperature dependent spectra. The computed spontaneous emission rate (see Fig. 3b and Eq. (4) of the main text) is shown with a green line for various temperatures. The main phonon modes responsible for the peaks are labeled, as well as the overtones ("o."). The peak broadenings as a function of temperature, as well as the effective "excitonic" temperatures, are discussed in the text. Black dots: experimental PL emission spectrum[11] (uncorrected for setup response). Blue squares: experimental CL emission spectrum.[12]

IV. TEMPERATURE DEPENDENCE

In our calculations, the temperature-dependent exciton lifetime, which is related to the imaginary part of the exciton-phonon self-energy and inversely proportional to the line broadenings η, remains an empirical parameter. As the imaginary part of our response functions intrinsically gives a Lorentzian shape for single peaks ($\mathrm{Im}[\omega - E - \mathrm{i}\eta]^{-1}$), we focus on the range of temperatures in which the experimental phonon-assisted peaks can also be reasonably described with a Lorentzian broadening (from 0 to 100 K).[11] We use a linear model where the line broadening η is given by[13]

$$\eta = \Gamma_0 + aT + bN_{BE}(T), \tag{S2}$$

where $N_{BE} = [\mathrm{e}^{E_O/kT} - 1]^{-1}$ is the Bose-Einstein distribution. The values of the parameters are taken from the experimental fit in Ref. [11]: $\Gamma_0 = 3$ meV, $a = 0.1$ meV/K, $b = 150$ meV, and $E_O = 25$ meV. For completeness, in Fig. S4 we provide a version of Fig. 3b of the main text with several temperatures (T= 8, 20, 60 and 100 K). The effective "excitonic" temperatures T_{exc} entering the Boltzmann factor of Eq. (4) of the main text are taken from the data points in Fig. 1c of Ref. [14]. At the lowest temperature ($5-8$ K, top frame), both the experimental spectra obtained from photoluminescence (PL, black dots, from Ref. [11]) and cathodoluminescence (CL, blue squares, from Ref. [12]) are compared with the computed one (green line). The temperature-dependent data are only available for the PL spectrum. Notice however that, contrary to the CL spectrum, the PL one is uncorrected for the response of the luminescence setup, giving rise to wrong relative peak intensities in the low-energy structure.

V. FORM OF THE FINITE-DIFFERENCE RESPONSE FUNCTION

Here we give the full derivation of Eqs. (2) and (3) of the main text. Let us consider the part of the response function due to excitonic state S (see Eq. (S1) for the full response function):

$$\chi_R^S(\omega) = \frac{|T_R^S|^2}{E_R^S - \hbar\omega + \mathrm{i}\eta}, \tag{S3}$$

where the subscript R denotes a parametric dependence on lattice displacements, i.e. χ_0^S is the frozen-atom response function (we take for simplicity η to be independent of R, an assumption that does not affect the validity of the results). We want to make the Taylor expansion of Eq. (S3) up to second order in the lattice displacements, therefore as an initial step we need to compute its first derivative and evaluate it at the equilibrium atomic positions:

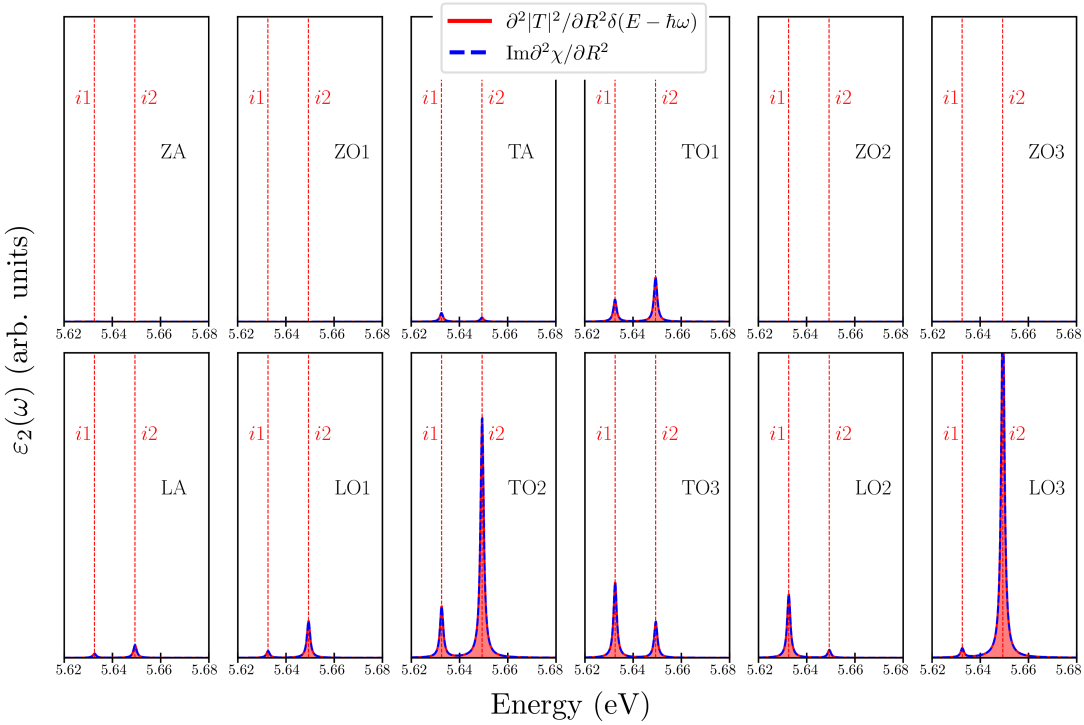

FIG. S5. Static exciton-phonon couplings between the $i1$ and $i2$ excitons and the 12 different phonons at $\overline{q} = \frac{1}{2}|\Gamma K|$. We compare results obtained from the full second derivative of the response function (dashed blue lines) and from the second derivative of the oscillator strengths (full red lines), see Eq. (S5). An average over polarization of the incoming light and sum over the 6 equivalent directions of phonons with wave vector $|\overline{q}|$ is performed.

$$\frac{\partial \chi_R^S(\omega)}{\partial R}\Big|_{R=0} = \frac{\partial |T_R^S|}{\partial R}\Big|_{R=0} 2|T_{R=0}^S|[E_{R=0}^S - \hbar\omega + \mathrm{i}\eta]^{-1} + \frac{\partial [E_R^S - \hbar\omega + \mathrm{i}\eta]^{-1}}{\partial R}\Big|_{R=0}|T_{R=0}^S|^2. \tag{S4}$$

At this point we notice that the oscillator strengths of any finite-q excitons for optical absorption must be zero because of momentum conservation. In the case of a supercell, it means that the excitons being folded into Γ from a different point in the unit cell are dark if the atoms are clamped at the equilibrium positions. If we label excitons belonging to such subset with S', this means that $T_{R=0}^{S'} = 0$ and therefore $\partial \chi_R^{S'}(\omega)/\partial R\Big|_{R=0} = 0$. This is explicitly confirmed numerically by our finite-difference calculations. This argument is analogous to the one often used in the case of optical absorption in the independent-particle model for the vanishing of the dipole optical matrix elements below the direct band gap.[15,16]

The same argument applied to the second derivative of χ_R^S leads to the vanishing of the terms containing derivatives of the exciton binding energy. The only term that remains is the one containing the second derivative of $T_R^{S'}$:

$$\frac{\partial^2 \chi_R^{S'}(\omega)}{\partial R^2}\Big|_{R=0} = \frac{\partial^2 |T_R^{S'}|^2}{\partial R^2}\Big|_{R=0} [E_{R=0}^{S'} - \hbar\omega + \mathrm{i}\eta]^{-1}, \tag{S5}$$

which corresponds to Eq. (3) of the main text. This derivative is evaluated numerically using the finite-difference expression

$$\partial^2 \chi_R/\partial R^2(\omega) \approx [\chi(\Delta\mathbf{R};\omega) - 2\chi_0(\omega) + \chi(-\Delta\mathbf{R};\omega)]/\Delta\mathbf{R}^2.$$

The results, displayed in Fig. S5 for each phonon mode, confirm the equivalence of the two sides of Eq. (S5). This means that, numerically, we can obtain the exciton-phonon coupling for the calculation of phonon-assisted absorption/emission both through a finite-difference calculation of the whole response function or through a finite-difference calculation of just the excitonic oscillator strength.

VI. EXCITON SYMMETRY AND COUPLING WITH PHONONS

A. Symmetry analysis with group theory

In bulk hBN, the point group (including the non-symmorphic point symmetry operations of the space

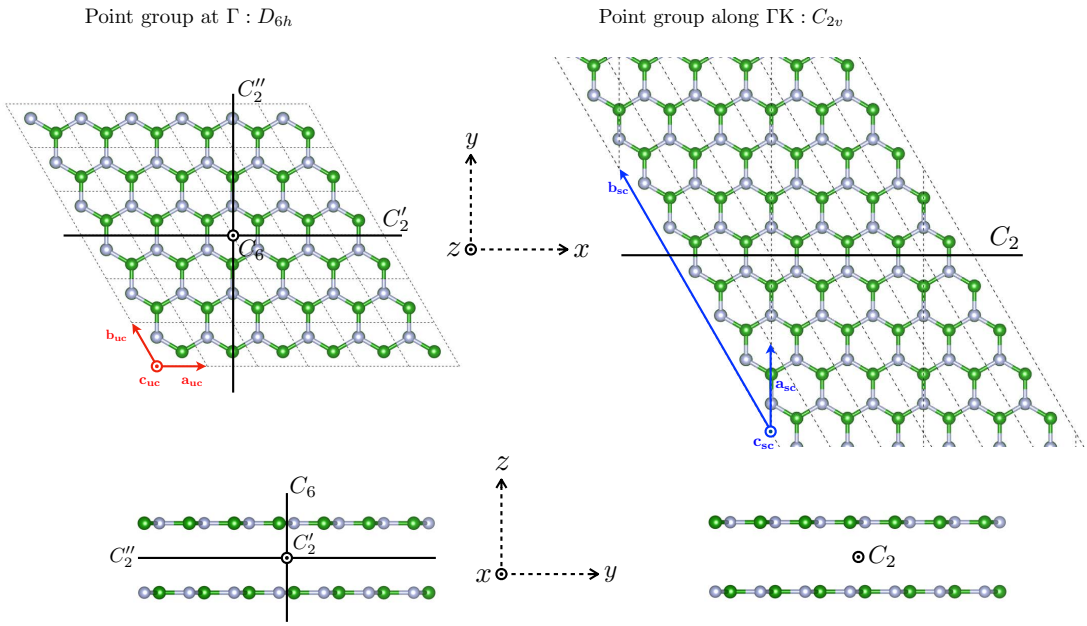

FIG. S6. Symmetries at Γ and $\overline{q}$. Top and side views of the bulk hBN lattice. Boron (nitrogen) atoms are in green (gray). The borders of the repeated unit cells are shown with dashed black lines. Left: original unit cell for the hexagonal lattice (D_{6h} point group) and lattice vectors. Right: non-diagonal supercell used in the calculations, folding point $\overline{q}$ (C_{2v} point group) at Γ, and lattice vectors. The axes of rotation corresponding to the symmetries of the q points of the systems are shown with solid black lines.

D_{6h}	E	$C_2'(x)$	$\sigma_h(xy)$	$\sigma_d(xz)$
A_{1g}	$+1$	$+1$	$+1$	$+1$
A_{2u}	$+1$	-1	-1	$+1$
E_{1g}	$+2$	0	-2	0
E_{2g}	$+2$	0	$+2$	0
E_{1u}	$+2$	0	$+2$	0
E_{2u}	$+2$	0	-2	0

TABLE I. Partial character table for point group D_{6h}.

C_{2v}	E	$C_2(x)$	$\sigma_v(xy)$	$\sigma_v(xz)$
A_1	$+1$	$+1$	$+1$	$+1$
A_2	$+1$	$+1$	-1	-1
B_1	$+1$	-1	$+1$	-1
B_2	$+1$	-1	-1	$+1$

TABLE II. Character table for point group C_{2v}.

D_{6h}		C_{2v}
C_2'	$\rightarrow$	C_2
$\sigma_h(xy)$	$\rightarrow$	$\sigma_v(xy)$
$\sigma_d(xz)$	$\rightarrow$	$\sigma_v(xz)$

TABLE III. Connection between the elements of C_{2v} and D_{6h}.

Mode	Symm.	Freq. (meV)
LO_3	A_1	183.00
LO_2	B_1	177.63
TO_3	A_1	159.58
TO_2	B_1	159.48
LA	A_1	93.33
LO_1	B_1	93.22
ZO_3	A_2	92.47
ZO_2	B_2	87.53
TO_1	A_1	65.10
TA	B_1	64.72
ZO_1	A_2	22.25
ZA	B_2	21.54

TABLE IV. Symmetry of the phonon modes at $\overline{q}$. The modes are listed as Davydov pairs in order of increasing frequency with the lowest-frequency mode at the bottom (compare Fig. (1) in the main text).

group) is D_{6h}. It contains 24 symmetry operations grouped in 12 classes. It is the group that is also used for the characterizations of perturbations (such as phonons and excitons) of hBN with zero wave-vector (corresponding to the high-symmetry point Γ). In Table I we report a subsection of the character table focusing on the operations and representations of interest to us. In Fig. S6 (left panel) our choice for the Cartesian axes and for the lattice vectors is reported and the three rota-

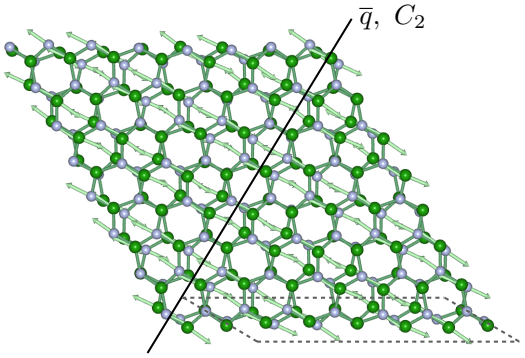

FIG. S7. Top view of the atomic displacements and forces for the TO_1 phonon mode at one of the six equivalent $\overline{q}$-vectors/C_2 rotation axes (solid black line). The corresponding non-diagonal supercell is represented in dashed gray lines.

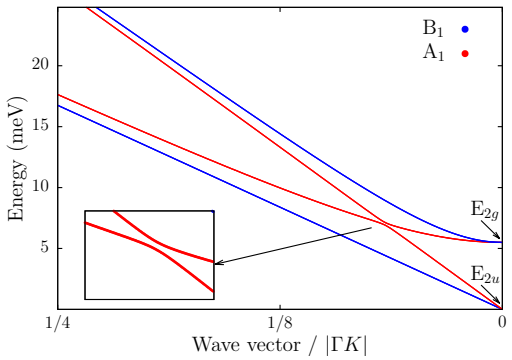

FIG. S8. Interplay between Davydov and symmetry splitting at very low wave vector for the transverse and longidutinal phonon modes (TA, TO_1, LA, LO_1 in the text). The dispersion of modes with symmetry A_1 (TO_1, LA) and B_1 (TA, LO_1) is shown in red and blue, respectively.

tion axes belonging to D_{6h} are drawn. Recall that bulk hBN displays AA′ stacking (two inequivalent layers per unit cell): therefore many of the symmetry operations are non-symmorphic. The point group for the symmetry analysis of a perturbation with finite wave vector $\overline{q}$ is a subset of the one at Γ. In the case of $\overline{q}$ lying on the ΓK line, the point symmetry group is C_{2v} with $C_{2v} \subset D_{6h}$. The character table of C_{2v} is provided in Table II. In the right panel of Fig. S6, showing the crystal lattice as repetitions of the non-diagonal supercell used in our calculations, the only rotation axis of C_{2v} is drawn. This axis runs along the zigzag direction, and it is identified by checking the rotational symmetry of the phonon modes, as shown in Fig. S8.[17] From this we see that the C_2 rotation in C_{2v} coincides with the C_2' rotation in D_{6h}, and we use this to make a connection between the elements of C_{2v} and D_{6h}, shown in Table III. The dipole operator transforms as the $[x, y, z]$ vector and belongs to representations $E_{1u}[x, y]+A_{2u}[z]$ for D_{6h} and $A_1[x]+B_1[y]+B_2[z]$ for C_{2v}. The in-plane component of the dipole transforms accordingly as E_{1u} and $A_1 + B_1$, respectively.

Let us first analyse the two excitons (one dark, one bright) of our system at Γ (see Fig. S3). The incoming optical light (E_{1u}) interacts with the ground state $|G\rangle$ of the system (which is fully symmetric, A_{1g}) creating an excited state of symmetry $A_{1g} \otimes E_{1u} = E_{1u}$. Therefore, the bright exciton corresponds to the E_{1u} representation. The dark state is its Davydov partner, thus it must have opposite parity with respect to inversion symmetry[7] and it corresponds to the E_{2g} representation, in analogy with the symmetry of the Davydov splitting for the acoustic phonons.

Any irreducible representation of D_{6h} will be a reducible representation of C_{2v}, and therefore can be expressed in terms of a linear combination of irreducible representations of C_{2v}. These are the so-called compatibility relations that we will need to analyse indirect processes from Γ to $\overline{q}$ (in particular, we want to describe the splitting of the E_{1u} and E_{2g} excitons). This applies also to the characters of the representations: if we define $\chi_{\mathcal{G}}(C_k)$ as the character of a (reducible) representation of group $\mathcal{G}$ with respect to symmetry operation C_k, the "wonderful orthogonality theorem" (according to Ref. 18) for characters establishes the coefficients a_{Γ_i} of the linear combination associated with irreducible representation Γ_i. In our case, the formulas reduce to

$$\chi_{D_{6h}}(C_k) = \sum_{\Gamma_i} a_{\Gamma_i} \chi^{(\Gamma_i)}_{C_{2v}}(C_k)$$

$$a_{\Gamma_i} = \frac{1}{4} \sum_k \chi^{(\Gamma_i)}_{C_{2v}}(C_k) \chi_{D_{6h}}(C_k),$$

and we can compute the a_{Γ_i} coefficients using the Tables I, II and III. We find $A_{2u} \to B_2$ and both E_{1u} and E_{2g} splitting as $A_1 + B_1$, confirming our previous identification of the dipole representations. Therefore, the two indirect excitons labeled as $i1$ and $i2$ with momentum $\overline{q}$ can only have either A_1 or B_1 symmetry.

B. Phonon symmetries and dispersion

We list in Table IV the results of our DFPT calculations for the symmetries of the phonon modes at $\overline{q}$. The formation of quasi-degenerate parallel phonon branches can be understood by zooming in on the region close to the Γ point as in Fig. S8. At Γ we see the two degenerate TA and LA modes (E_{2u} symmetry) at zero frequency, as well as their Davydov partner (TO_1 and LO_1 modes, E_{2g} symmetry) 6 meV above. The large value of the splitting is due to the constructive interference of the Fourier components of the inter-layer interaction at zero wave vector. When $q \neq 0$, the degenerate modes further split into two non-degenerate ones of symmetry A_1 and B_1. The two A_1 modes mix via an avoided crossing and then approach their respective B_1 mode. In this way two distinct Davydov pairs are formed, each one with a tiny energy split-

ting. The low value of the splitting at finite q is due to the destructive interference of the Fourier components of the inter-layer interaction.

C. Selection rules for indirect absorption

In order to analyse the indirect process, we first list in Table IV the results of our DFPT calculations for the symmetries of the phonon modes at $\overline{q}$. Next we consider the time-dependent perturbation theory for a model excitonic Hamiltonian H_0 with exciton-radiation and exciton-lattice interactions as the perturbations: $H = H_0 + V(t) = H_0 + D\mathrm{e}^{-\mathrm{i}\omega t} + g_{\overline{q}}\mathrm{e}^{-\mathrm{i}\Omega_{\overline{q}}t} + h.c.$, where ω and $\Omega_{\overline{q}}$ are the photon and phonon frequencies, respectively, and D and $g_{\overline{q}}$ the coupling operators (a sum over all phonon modes is assumed). We want to qualitatively describe the phonon-assisted processes leading to the formation or annihilation of a finite-q excitonic state $|\psi_f\rangle$. We include only single-photon and single-phonon processes, and for simplicity we only consider phonon emission contributions. (Note that the following derivation is not meant to give a precise computational description of indirect absorption but that it serves only for the symmetry analysis of the involved phonons and excitons). Then we can write the second-order Fermi golden rule expression for the transition probability per unit time as[19]

$$\begin{aligned} P_f^{II} = \frac{2\pi}{\hbar}\left|\sum_\alpha \frac{\langle\psi_f|\, g_{\overline{q}}^\dagger\,|\psi_\alpha\rangle\,\langle\psi_\alpha|\, D\,|G\rangle}{E_\alpha - \hbar\omega} + \sum_{\alpha'} \frac{\langle\psi_f|\, D\,|\psi_{\alpha'}\rangle\,\langle\psi_{\alpha'}|\, g_{\overline{q}}^\dagger\,|G\rangle}{E_{\alpha'} - \hbar\Omega_{\overline{q}}}\right|^2 \delta(E_f - \hbar\omega + \hbar\Omega_{\overline{q}}) + \\ \frac{2\pi}{\hbar}\left|\sum_\alpha \frac{\langle\psi_f|\, g_{\overline{q}}^\dagger\,|\psi_\alpha\rangle\,\langle\psi_\alpha|\, D^\dagger\,|G\rangle}{E_\alpha + \hbar\omega} + \sum_{\alpha'} \frac{\langle\psi_f|\, D^\dagger\,|\psi_{\alpha'}\rangle\,\langle\psi_{\alpha'}|\, g_{\overline{q}}^\dagger\,|G\rangle}{E_{\alpha'} - \hbar\Omega_{\overline{q}}}\right|^2 \delta(E_f + \hbar\omega + \hbar\Omega_{\overline{q}}). \end{aligned} \tag{S6}$$

Here $|\psi_\alpha\rangle$ is an intermediate excitonic state with energy E_α and $|G\rangle$ is the ground state of the system. The first term corresponds to the process of photon absorption with phonon emission creating the final excitonic state $|\psi_f\rangle$, while the second term describes the combined photon and phonon emission. We notice immediately that if we take the static approximation for the transition probabilities (i.e. setting $\hbar\omega = \hbar\Omega_{\overline{q}} = 0$ in the denominators) and $D = D^\dagger$ (e.g. the dipole operator), the squared quantities coincide for both photon absorption and emission. This is the limit in which we performed our finite-difference calculations and is analogous to the Hall-Bardeen-Blatt theory of indirect absorption for independent particles.[15] The first term in the squared sum represents the creation of a direct virtual exciton $|\psi_\alpha\rangle$ by light as the intermediate step, followed by a scattering to the finite-q state $|\psi_f\rangle$ via phonon emission. The second term adds the contribution of the inverse process, when the virtual state $|\psi_{\alpha'}\rangle$ is created at finite-q by a phonon, and then arrives at the energy of $|\psi_f\rangle$ by absorbing a photon. For the purposes of finding the selection rules, the two contributions are equivalent and thus we focus on the first one, $\langle\psi_f|\, g_{\overline{q}}^\dagger\,|\psi_\alpha\rangle\,\langle\psi_\alpha|\, D\,|G\rangle$. The final allowed excitons in the energy window that we consider must have A_1 and B_1 symmetry and the first matrix element in the process, $\langle\psi_\alpha|\, D\,|G\rangle$, imposes E_{1u} as the only possible representation for the direct intermediate state $|\psi_\alpha\rangle$. Since $E_{1u} \to A_1 + B_1$ and $g_{\overline{q}}^\dagger$ transforms with the symmetry of the various phonon modes involved, for $g_{\overline{q}}^\dagger\,|\psi_\alpha\rangle$ we have the tensor product $(A_1{+}B_1{+}A_2{+}B_2){\otimes}(A_1{+}B_1)$. However, $A_1{\otimes}(A_2{+}B_2) = A_2 + B_2$ and $B_1 \otimes (A_2 + B_2) = B_2 + A_2$, therefore the phonon modes transforming as A_2 or B_2 cannot give the allowed final states and their coupling is forbidden. We see from Table IV that these representations correspond to the out-of-plane Z phonon modes, while the in-plane ones T and L all transform as A_1 or B_1 and therefore are all allowed. If we consider instead incoming light polarised out-of-plane ($A_{2u} \to B_2$), the picture changes and now $(A_1{+}B_1{+}A_2{+}B_2){\otimes}B_2 = B_2{+}A_2{+}B_1{+}A_1$, meaning that if the polarization is exclusively out-of-plane only the Z phonon modes can couple to excitons $i1$ and $i2$.

We find that our first-principles calculations respect the aforementioned selection rules, as shown in Fig. S9. In particular, *if light is polarzsed exclusively along the x/zigzag direction*, i.e., it transforms as A_1 (top frame), then only the TA, LO_1, TO_2 and LO_2 phonon modes (all transforming as B_1, portrayed in blue) can couple to $i1$ forming phonon-assisted peaks, and only the TO_1, LA, TO_3 and LO_3 modes (all transforming as A_1, portrayed in red) can couple to $i2$. Conversely, *if light is polarized exclusively along the y/armchair direction*, i.e., it transforms as B_1 (bottom frame), then only the A_1 phonon modes couple with $i1$, and only the B_1 modes couple with $i2$. This unmistakably shows that exciton $i1$ (the one responsible for the luminescence spectrum) has B_1 symmetry, while exciton $i2$ transforms as A_1. Additionally, we notice that the leading peak for absorption is due solely to the strong coupling between the $i2$ exciton and the LO_3 phonon mode: therefore, this peak completely disappears when light is polarised along the y direction (that is, orthogonal to the $\overline{q}$ vector). Finally, we confirm that the total spectrum is $\pi/3$-periodic by varying the light polarization direction.

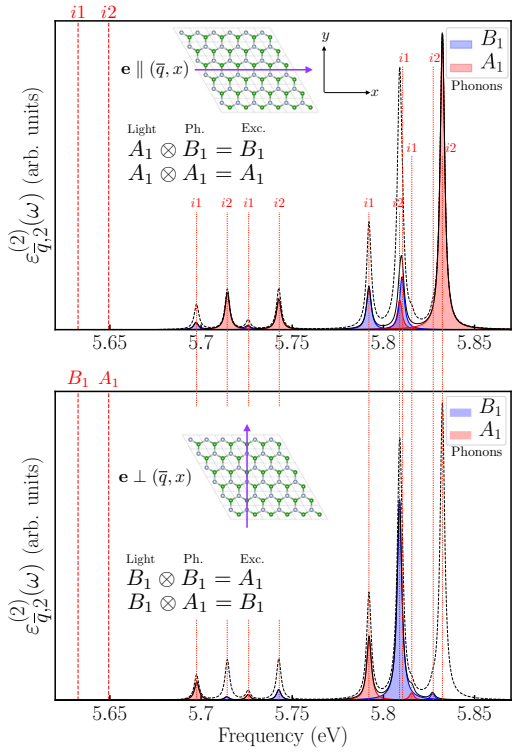

FIG. S9. *Ab initio* results on exciton-phonon coupling, resolved by direction of light-polarization and symmetry of contributing phonon modes. The contribution to absorption, assisted by a phonon of wave vector $\bar{q}$ along the x-direction is plotted (solid black line) for light polarization $\mathbf{e}$ along the x-direction (top frame) and the y-direction (bottom frame). The dashed black line represents the full result obtained by averaging over the two contributions. The red vertical lines serve as a guide for the eyes to understand which phonon-assisted peaks come from the coupling to excitons $i1$ or $i2$. The color of each phonon-assisted peak indicates the symmetry of the phonon mode responsible for it (B_1: blue, A_1: red).

VII. VAN ROOSBROECK-SHOCKLEY RELATION

We give here a short account of the van Roosbroeck-Shockley (RS) relation,[20] in order to add some context to its application to our results (Eq. (4) of the main text). We mainly adapt the contents of Refs. [21] and [22], where a more exhaustive treatment can be found.

Direct transitions in the independent-particle case. Let us consider a steady state of photon absorption and emission processes between valence and conduction bands. For simplicity of notation, the photon polarizations are not included. The net absorption rate (per unit energy, per unit volume) will be given by the difference between the transition rates of absorption and stimulated emission processes:

$$R'_{\rm abs}(\omega) = \mathcal{K}(\omega)\frac{2\pi}{\hbar}\frac{\mathcal{N}(\omega)}{N_k}\sum_{cvk}\mathcal{T}_{cvk}\Delta^{F\prime}_{cvk}\delta(\epsilon_{ck}-\epsilon_{vk}-\hbar\omega), \tag{S7}$$

where ϵ_{nk} is the energy of an electron in the nth band with wave vector k, $\mathcal{T}_{cvk}$ is the transition rate and $\Delta^{F\prime}_{cvk} = n^F_{vk}n^{F\prime}_{ck} - n^F_{ck}n^{F\prime}_{vk}$. Here, n^F_{nk} is the probability that state ϵ_{nk} is occupied with an electron, and $n^{F\prime}_{nk}$ the probability that it is occupied with a hole. We assume a time-independent Fermi-Dirac distribution for electronic occupations in the steady state, $n^F_{nk} = [1+\mathrm{e}^{(\epsilon_{nk}-\mu_e)/kT}]^{-1}$, with μ_e and μ_h being the chemical potentials for electrons and holes, respectively. In the independent-particle case the transition rate can be taken as the optical matrix element in the dipole approximation: $\mathcal{T}_{cvk} = |\langle ck|\hat{D}|vk\rangle|^2$. We can similarly write the expression for the spontaneous emission rate,

$$R^{sp}(\omega) = \mathcal{K}(\omega)\frac{2\pi}{\hbar}\frac{\mathcal{G}(\omega)}{N_k}\sum_{cvk}\mathcal{T}_{cvk}n^F_{ck}n^{F\prime}_{vk}\delta(\epsilon_{ck}-\epsilon_{vk}-\hbar\omega). \tag{S8}$$

The spontaneous emission is only proportional to the photon density of states, $\mathcal{G}(\omega)$, while both absorption and stimulated emission are proportional to the the photon density per unit energy, $\mathcal{N}(\omega)$. If we define an average photon number, $\overline{\mathcal{N}}$, these two quantities are related by the total photon density $\int\mathcal{N}(\omega)\mathrm{d}\omega = \int\overline{\mathcal{N}}\mathcal{G}(\omega)\mathrm{d}\omega$. The dimensional term $\mathcal{K}(\omega)$ is made of quantities mainly related to the the electro-magnetic field. It is important to notice that this term is also frequency-dependent. We now list the expressions for the optical quantities involved.

$$\text{Dimensional factor}\quad \mathcal{K}(\omega) = \frac{2\pi e^2\hbar^2}{m^2V}\frac{1}{n_r(\omega)^2\hbar\omega}$$

$$\text{Photon density of states}\quad \mathcal{G}(\omega) = \frac{1}{\pi^2c^2\hbar^3}\frac{n_r(\omega)^2(\hbar\omega)^2}{V_g(\omega)}$$

$$\text{Group velocity}\quad V_g(\omega) = \frac{c}{n_r(\omega)+\omega\frac{\partial n_r(\omega)}{\partial\omega}} \approx \frac{c}{n_r(\omega)}$$

$$\text{Incoming photon flux}\quad \mathcal{F}(\omega) = \mathcal{N}(\omega)\frac{c}{n_r(\omega)}$$

The absorption coefficient $\alpha(\omega)$ can be written in terms of the absorption rate as $R'_{\rm abs}(\hbar\omega) = \mathcal{F}(\omega)\alpha(\omega)$. Finally, we observe that independently from the specific (cvk) transition considered, the following relation always holds:

$$\frac{n^F_{ck}n^{F\prime}_{vk}}{n^F_{vk}n^{F\prime}_{ck} - n^F_{ck}n^{F\prime}_{vk}} = \frac{1}{\mathrm{e}^{(\hbar\omega-(\mu_e-\mu_h))/kT}-1} \approx \mathrm{e}^{-(\hbar\omega-\Delta\mu)/kT}$$

Then, by putting everything together and comparing Eqs. (S7) and (S8), we find $R_{\rm sp}(\omega) = \mathcal{G}(\omega)V_g(\omega)\alpha(\omega)\mathrm{e}^{-(\hbar\omega-\Delta\mu)/kT}$.

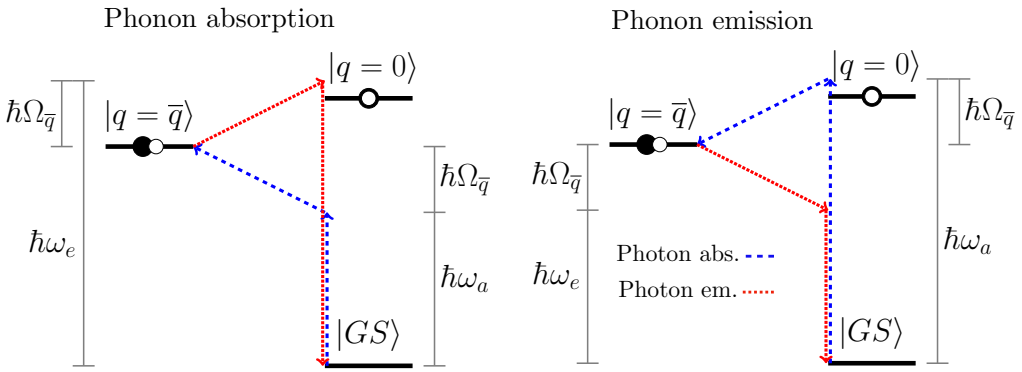

FIG. S10. Simplified two-exciton scheme for hBN, displaying the processes of photon absorption (dashed blue arrows) and emission (dotted red arrows) mediated by phonon absorption (left) and phonon emission (right).

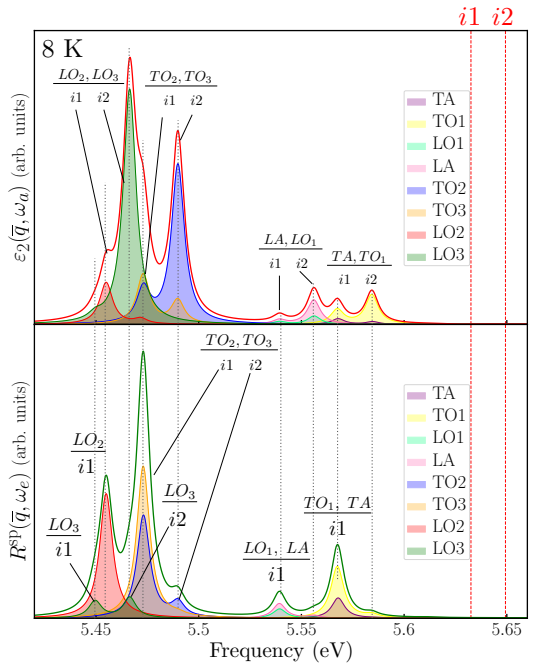

FIG. S11. Phonon-assisted emission in bulk hexagonal boron nitride. Spectral functions $\varepsilon_2(\overline{q},\omega_a) = \sum_\lambda \varepsilon_{2\lambda}^{\rm exc}(\overline{q},\omega_a)$ (red, top, $\mathrm{Im}\varepsilon_{\overline{q}}^{em}(\omega)$ in the main text) and $R^{\rm sp}(\overline{q},\omega_e) = \sum_\lambda R_\lambda^{\rm sp}(\overline{q},\omega_e)$ (green, bottom, $R_{\overline{q}}^{\rm sp}(\omega)$ in the main text) at 8 K. The λ-components of the spectrum, belonging to the different phonon modes, are also plotted in various colours. The exciton-phonon couplings are labeled. The dotted vertical lines in correspondence with the peaks serve as a guide for the eyes.

This leads us to the RS relation:

$$R_{\rm sp}(\omega) = \frac{n_r(\omega)^2(\hbar\omega)^2}{\pi^2c^2\hbar^3}\alpha(\omega)\mathrm{e}^{-(\hbar\omega-\Delta\mu)/kT} = \frac{n_r(\omega)(\hbar\omega)^3}{\pi^2c^3\hbar^4}\varepsilon_2(\omega)\mathrm{e}^{-(\hbar\omega-\Delta\mu)/kT}, \tag{S9}$$

where for the last equality we have used $\alpha(\omega) = \hbar\omega\varepsilon_2(\omega)/(n_r(\omega)\hbar c)$.

Direct transitions in the exciton case. In this case the absorption coefficient is computed including excitonic effects ($\alpha^{\rm exc}(\omega)$ or equivalently $\varepsilon_2^{\rm exc}(\omega)$; we can always obtain the full refractive index as $n_r^{\rm exc}(\omega) = \sqrt{(\sqrt{\varepsilon_1^{\rm exc}(\omega)^2+\varepsilon_2^{\rm exc}(\omega)^2}+\varepsilon_1^{\rm exc}(\omega))/2}$). This means that the transition rate $\mathcal{T}_{cvk}$ in Eqs. (S7) and (S8) will be replaced by the excitonic one, $\mathcal{T}_S = |\sum_{cvk}\Phi_{cvk}^S\langle ck|\,\hat{p}\,|vk\rangle|^2$, with the external sum now running over the exciton index S. Analogously, the energies of single-particle transitions will be replaced by the exciton energy levels E^S. Concerning the occupation functions, if the absorption/emission features are dominated by the creation/annihilation of electron-hole bound pairs, it is sufficient to replace the Bose-Einstein/Boltzmann factor in Eq. (S9) with a more appropriate term to describe the occupation of excitonic states. We use the Boltzmann distribution $N_B(\hbar\omega) = \mathrm{e}^{-(\hbar\omega-\mu^*)/kT}$, with μ^* fixed to the energy of the lowest-bound exciton. Since below the quasiparticle gap we are dealing with a discrete excitonic spectrum, N_B will be a discrete function taking values for $\hbar\omega = E^S$.

Indirect transitions. In this case we have to take into account that the energy of a photon absorbed ($\hbar\omega_a$) and that of a photon emitted ($\hbar\omega_e$) in a process mediated by the same phonon are not the same, and they are both different from the energy of the electronic transition ($\hbar\omega$). In particular, with the help of Fig. S10, we can write the following relations: $\hbar\omega_e = \hbar\omega_a \pm 2\hbar\Omega_\lambda$, $\hbar\omega_e = \hbar\omega \pm \hbar\Omega_\lambda$ and $\hbar\omega_a = \hbar\omega \mp \hbar\Omega_\lambda$, where Ω_λ is the frequency of the phonon assisting the transition and the upper and lower signs refer to the cases of phonon absorption and emission, respectively. We need to write a generalised form of the RS relation that takes these energy differences into account. Focusing on the case of an indirect transition mediated by the emission of a single phonon of branch λ and momentum q, the second-order absorption and emission rates (i.e. per unit time, energy and volume) can be

expressed as (back in the independent-particle case)

$$
\begin{aligned}
R'_{\rm abs}(\omega_a) &= \mathcal{K}(\omega_a)\frac{2\pi}{\hbar}\frac{\mathcal{N}(\omega_a)}{N_k}\sum_{cvk}\mathcal{T}^{(2)}_{cvkq\lambda}(n_{q\lambda}+1)[n^F_{vk}n^{F\prime}_{ck+q}-n^F_{ck+q}n^{F\prime}_{vk}]\delta(\epsilon_{ck+q}-\epsilon_{vk}+\hbar\Omega_{q\lambda}-\hbar\omega_a)\\
R^{sp}(\omega_e) &= \mathcal{K}(\omega_e)\frac{2\pi}{\hbar}\frac{\mathcal{G}(\omega_e)}{N_k}\sum_{cvk}\mathcal{T}^{(2)}_{cvkq\lambda}(n_{q\lambda}+1)n^F_{ck+q}n^{F\prime}_{vk}\delta(\epsilon_{ck+q}-\epsilon_{vk}-\hbar\Omega_{q\lambda}-\hbar\omega_e),
\end{aligned}
\tag{S10}
$$

where $n_{q\lambda}$ represents the Bose-Einstein distribution for phonons (we use n_B in the main text).

Then, considering $\alpha(\hbar\omega_a) = R'_{\rm abs}(\hbar\omega_a)/\mathcal{F}(\hbar\omega_a)$ and writing the frequency-dependent functions explicitly, we can write the final results:

$$
\begin{aligned}
R^{sp}(\omega_e) &= \frac{n_r(\omega_e)n_r(\omega_a)(\hbar\omega_e)(\hbar\omega_a)}{\pi^2c^2\hbar^3}\alpha(\omega_a)\mathrm{e}^{-(\hbar\omega-\Delta\mu)/kT}\\
&= \frac{n_r(\omega_e)(\hbar\omega_e)(\hbar\omega_a)^2}{\pi^2c^3\hbar^4}\varepsilon_2(\omega_a)\mathrm{e}^{-(\hbar\omega-\Delta\mu)/kT}.
\end{aligned}
\tag{S11}
$$

Or, in the excitonic case (dropping the labels on the frequencies): $R^{sp}(\omega) \propto n_r^{\rm exc}(\omega)\omega(\omega-2\Omega_{q\lambda})^2\varepsilon_2^{\rm exc}(\omega-2\Omega_{q\lambda})N_B$. The emission spectra shown in Fig. 3 of the main text are obtained by using the latter equation (Eq. (4) in the main text) and summing over all phonon modes with momentum $q=\overline{q}$ corresponding to the indirect gap. Using our *ab initio* results, a comparison between $\varepsilon_2(\overline{q},\hbar\omega_a)$ (where all phonon-assisted peaks are simply mirrored with respect to the energy of the excitonic state involved) and $R^{sp}(\hbar\omega_e)$, the full RS relation, is shown in Fig. S11.

[1] J. H. Lloyd-Williams and B. Monserrat, Phys. Rev. B **92**, 184301 (2015).
[2] P. Giannozzi, S. Baroni, N. Bonini, M. Calandra, R. Car, C. Cavazzoni, D. Ceresoli, G. L. Chiarotti, M. Cococcioni, I. Dabo, A. D. Corso, S. de Gironcoli, S. Fabris, G. Fratesi, R. Gebauer, U. Gerstmann, C. Gougoussis, A. Kokalj, M. Lazzeri, L. Martin-Samos, N. Marzari, F. Mauri, R. Mazzarello, S. Paolini, A. Pasquarello, L. Paulatto, C. Sbraccia, S. Scandolo, G. Sclauzero, A. P. Seitsonen, A. Smogunov, P. Umari, and R. M. Wentzcovitch, J. Phys. Condens. Matter **21**, 395502 (2009).
[3] J. P. Perdew and A. Zunger, Phys. Rev. B **23**, 5048 (1981).
[4] M. Fuchs and M. Scheffler, Computer Physics Communications **119**, 67 (1999).
[5] S. Baroni, S. de Gironcoli, A. Dal Corso, and P. Giannozzi, Rev. Mod. Phys. **73**, 515 (2001).
[6] D. Sangalli, A. Ferretti, H. Miranda, C. Attaccalite, I. Marri, E. Cannuccia, P. M. Melo, M. Marsili, F. Paleari, A. Marrazzo, G. Prandini, P. Bonf, M. O. Atambo, F. Affinito, M. Palummo, A. M. Sanchez, C. Hogan, M. Grning, D. Varsano, and A. Marini, Journal of Physics: Condensed Matter (2019).
[7] F. Paleari, T. Galvani, H. Amara, F. Ducastelle, A. Molina-Sánchez, and L. Wirtz, 2D Materials **5**, 045017 (2018).
[8] V. Hernandez, J. E. Roman, and V. Vidal, ACM Trans. Math. Softw. **31**, 351 (2005).
[9] G. Onida, L. Reining, and A. Rubio, Rev. Mod. Phys. **74**, 601 (2002).
[10] B. Arnaud, S. Lebègue, P. Rabiller, and M. Alouani, Phys. Rev. Lett. **96**, 026402 (2006).
[11] T. Q. P. Vuong, G. Cassabois, P. Valvin, S. Liu, J. H. Edgar, and B. Gil, Phys. Rev. B **95**, 201202 (2017).
[12] L. Schué, L. Sponza, A. Plaud, H. Bensalah, K. Watanabe, T. Taniguchi, F. m. c. Ducastelle, A. Loiseau, and J. Barjon, Phys. Rev. Lett. **122**, 067401 (2019).
[13] S. Rudin, T. L. Reinecke, and B. Segall, Phys. Rev. B **42**, 11218 (1990).
[14] G. Cassabois, P. Valvin, and B. Gil, Nat. Photonics **10**, 262 (2016).
[15] L. H. Hall, J. Bardeen, and F. J. Blatt, Phys. Rev. **95**, 559 (1954).
[16] M. Zacharias and F. Giustino, Phys. Rev. B **94**, 075125 (2016).
[17] We used the following online tool to visualise the phonon dispersion and lattice displacements corresponding to different q-vectors: `http://henriquemiranda.github.io/phononwebsite/phonon.html`.
[18] M. S. Dresselhaus, G. Dresselhaus, and A. Jorio, *Group theory: Application to the Physics of Condensed Matter* (Springer, 2008).
[19] F. Bassani and G. P. Parravicini, *Electronic States and Optical Transition in Solids* (Oxford: Pergamon, 1975) Chap. XII. Optical properties of semiconductors and insulators.
[20] W. van Roosbroeck and W. Shockley, Phys. Rev. **94**, 1558 (1954).
[21] P. T. Landsberg, *Recombination in semiconductors* (Cambridge University Press, 1991) Chap. Radiative recombination (mainly for bands).
[22] H. B. Bebb and E. W. Williams, *Semiconductors and semimetals* (Elsevier, 1972) Chap. Photoluminescence I: Theory.